J Solid State Electrochem (1997) 1: 45–52

ORIGINAL PAPER

Li-Jun Wan · Shueh-Lin Yau · Kingo Itaya

Structure of thiocyanate adlayers on Rh(111): an in situ STM study

Received: 26 February 1997 / Accepted: 3 March 1997

Abstract In situ scanning tunneling microscopy (STM) was used to examine the structure of thiocyanate adlayers specifically adsorbed on Rh(111) in solutions of potassium hydroxide and perchloric acid, both containing potassium thiocyanate (KSCN). An atomically flat terrace-step structure was consistently observed on Rh(111) surfaces prepared by the flame-annealing-quenching method. The Rh(111)-(1×1) atomic structure was discerned on the atomically flat terrace even in the alkaline solution. High-resolution STM images disclosed two different structures of the SCN^- adlayers, $(2 \times \sqrt{3})$ and (2×2), in the alkaline and the acidic media, respectively. In each structure, an individual adsorbed SCN^- ion appeared as a single spot with a constant corrugation height in STM images, suggesting that SCN^- ions adsorbed predominantly with their S-ends at particular bonding sites on Rh(111). The difference in the adlayer structure in the two solutions can be attributed to the interaction between adsorbed SCN^- and coadsorbed K^+ in the alkaline solution, and is different from that between adsorbed SCN^- and H^+ in the acidic solution.

Key words In situ STM · Rh(111) · Thiocyanate · Adlayer structure

Introduction

In situ scanning tunneling microscopy has made it possible to elucidate structures of adlayers as well as the role of specifically adsorbed anions in various electrochemical reactions such as dissolution and deposition on an atomic scale. For example, the adlayer structure of anions such as I^- [1–4], Br^- [5], CN^- [6, 7], and sulfate/bisulfate [8, 9] has been intensively investigated, mainly on Pt(111) and Au(111). The effects of adsorbed anions on the dissolution of metals such as Pd [10, 11], Ni [12], Cu [13, 14], and Ag [15] have also recently been described based on in situ STM.

In spite of a large number of investigations of these metal electrodes, few papers addressing the adsorption of anions on Rh electrodes are to be found in the literature [16, 17]. Hourani and Wieckowski first described a systematic voltammetric study of an ordered Rh(111) in electrolyte solutions containing various anions [16]. Adlayer structures of iodine and CO on Rh(111) were determined using an ultrahigh vacuum-electrochemical approach (UHV-EC) [17]. It is known that the electroreduction of perchlorate is one of the most characteristic properties of Rh electrodes [18–20].

Recently, we demonstrated that an in situ STM approach could determine the structures of I^- and sulfate/bisulfate adsorbed on the well-defined Rh(111) [21, 22]. The well-defined terrace-step structure can be easily exposed in solution by the flame-annealing-quenching method. More recently, ordered structures of organic molecules such as benzene have been determined on Rh(111) in solution by in situ STM [23]. Less ordered benzene adlayers were found to form on Pt(111) [23]. These experimental results strongly encouraged us to investigate adlayer structures of various chemical species formed on Rh(111).

The absorption of thiocyanate anions (SCN^-) is one of the most intensively investigated subjects using various experimental techniques. Vibrational spectroscopic techniques such as infrared absorption spectroscopy (IR) have been employed for studying SCN^- adsorbed on various electrodes such as Pt, Au, and Ag [24–30]. Ex situ STM was also recently used to examine the structure of SCN^- on Au(111) in air, revealing a square atomic pattern [31]. As a result of these studies, it is

L.-J. Wan (✉) · S.-L. Yau
Itaya Electrochemiscopy Project, ERATO/JST,
The Research Institute of Electric and Magnetic Materials,
2-1-1 Yagiyama-minami, Sendai 980, Japan

K. Itaya
Department of Applied Chemistry, Faculty of Engineering,
Tohoku University, Sendai 980, Japan
Tel.: +81-22-214-5380; Fax: +81-22-214-5380;
e-mail: itaya@atom.che.tohoku.ac.jp

generally believed that the linear SCN^- ion is bound to the metal surface via the S end at least within the potential range of double layer charging. At more negative potentials, the adsorbed SCN^- anion may become bound to the metal through the N end, as has been suggested by an in situ IR study on a polycrystalline Pt electrode [30]. UHV-EC has been used to examine the structures of adsorbed SCN^- layers on Pt(111) and Ag(111) electrodes [32–34]. Hubbard and coworkers first reported a (2×2)-2SCN structure on Pt(111) [32, 33], and more recently a (1×2)-SCN structure [34], indicating some complicating factors in the formation of SCN^- adlayers, even on Pt(111). Besides the adlayer structures, high-resolution electron energy-loss spectroscopy (HREELS) results indicated the coexistence of N-bound as well as S-bound species, the latter being predominant [34]. Our recent preliminary in situ STM study [35] of SCN^- on Pt(111) revealed a potential dependence of STM images and two different (2×2) structures at cathodic potentials. The observation of (2×2) symmetry is consistent with that found in UHV [32, 33]. However, no detailed investigation had hitherto been carried out for the SCN^- adlayer on Rh electrodes.

In the present study, the adlayer structure of SCN^- on Rh(111) was investigated by in situ STM in solutions of KOH and $HClO_4$, both containing KSCN. We demonstrated that adlayer structures were dependent on pH of solutions. The structure was not affected by changing the electrode potential, at least in the double layer potential range.

Experimental

The method of preparation of the Rh single-crystal electrode has already been described elsewhere [21–23]. Briefly, an Rh wire (0.5 mm in diameter) was melted in H_2/O_2 mixed flame. The crystallization of the Rh single-crystal bead was indicated by the appearance of eight properly arranged (111) facets. These (111) facets usually gave atomically flat terrace-step structures. For voltammetric measurements, a (111) facet was mechanically exposed and polished with successively finer grades of Al_2O_3 powder, from 1 μm to 0.05 μm in diameter. The Rh(111) electrode was finally annealed using an H_2/O_2 torch for at least 30 min to remove surface damage caused by mechanical polishing. A flame-annealing-quenching procedure was used to prepare a well-defined, oxide-free Rh(111) surface using hydrogen-saturated pure water. After the annealing-quenching treatment, the Rh electrode, with the surface protected by a droplet of water, was quickly transferred to an electrochemical cell containing a solution.

All solutions were prepared with KSCN, $HClO_4$, KOH (Merck, p. a. grade) and ultrapure water (Millipore-Q). Cyclic voltammetry was performed in a three-chamber cell with a reversible hydrogen reference electrode (RHE) in the same electrolyte solution containing no KSCN and a Pt counter electrode. All electrochemical potentials are reported with respect to the RHE.

In situ STM images were obtained with a Nanoscope III scanning tunneling microscope (Digital Instruments, Santa Barbara, Calif.). A modified STM cell with an RHE and a Pt counter electrode was used. The STM tips were prepared by electrochemically etching a tungsten wire (0.25 mm in diameter) with an AC voltage of 15 V in 0.6 M KOH. The W tips were then coated with transparent nail polish to minimize the faradaic current. These W tips have been used successfully for achieving atomic resolution in situ STM images. All STM images were taken in the constant-current mode.

Results and discussion

Cyclic voltammetry

Figure 1 shows a typical cyclic voltammogram (CV) of an Rh(111) electrode in 0.1 M $HClO_4$. The so-called butterfly peak at 0.64 V can be found only with a well-defined Rh(111) surface. No such peak appeared with even a slightly disordered surface, as described previously [21]. A very sharp peak at 0.06 V, whose height strongly depended on the quality of the surface of Rh(111), is also characteristic. The asymmetric feature in the hydrogen adsorption and desorption region is due to the electroreduction of perchlorate to chloride ions, which are expected to be adsorbed on the electrode, resulting in a complex surface composition. Note that almost completely symmetric features were observed on Rh(111), both for the hydrogen adsorption-desorption peaks and for the butterfly peak in HF solution, as described previously [23]. Nevertheless, the overall shape of the CV shown in Fig. 1 is consistent with that observed previously in $HClO_4$ [18–22].

To our knowledge, there is no previous voltammetric study of Rh(111) in alkaline medium, although the hydrogen adsorption-desorption was previously investigated on polycrystalline Rh electrodes [36, 37]. Figure 2a shows CV curves obtained with a well-defined Rh(111) in 0.1 M KOH in a cathodic potential range at various scanning rates. The shape of the CV was not altered by repeated potential cycles in the potential range 0–0.95 V for at least 1 h, indicating that the well-

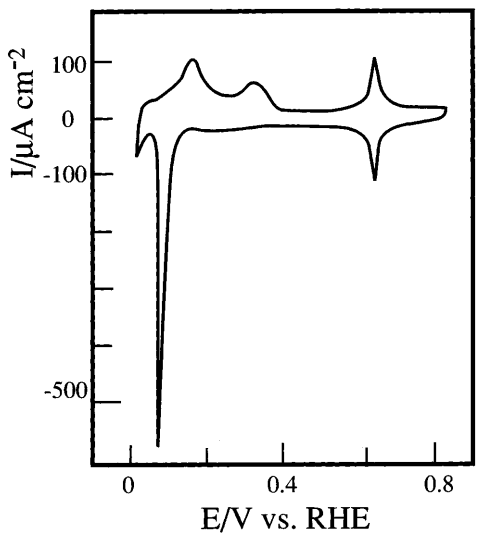

Fig. 1 Cyclic voltammogram for Rh(111) in 0.1 M $HClO_4$. The potential scan rate was 50 mV/s. The first scan was made in the cathodic direction

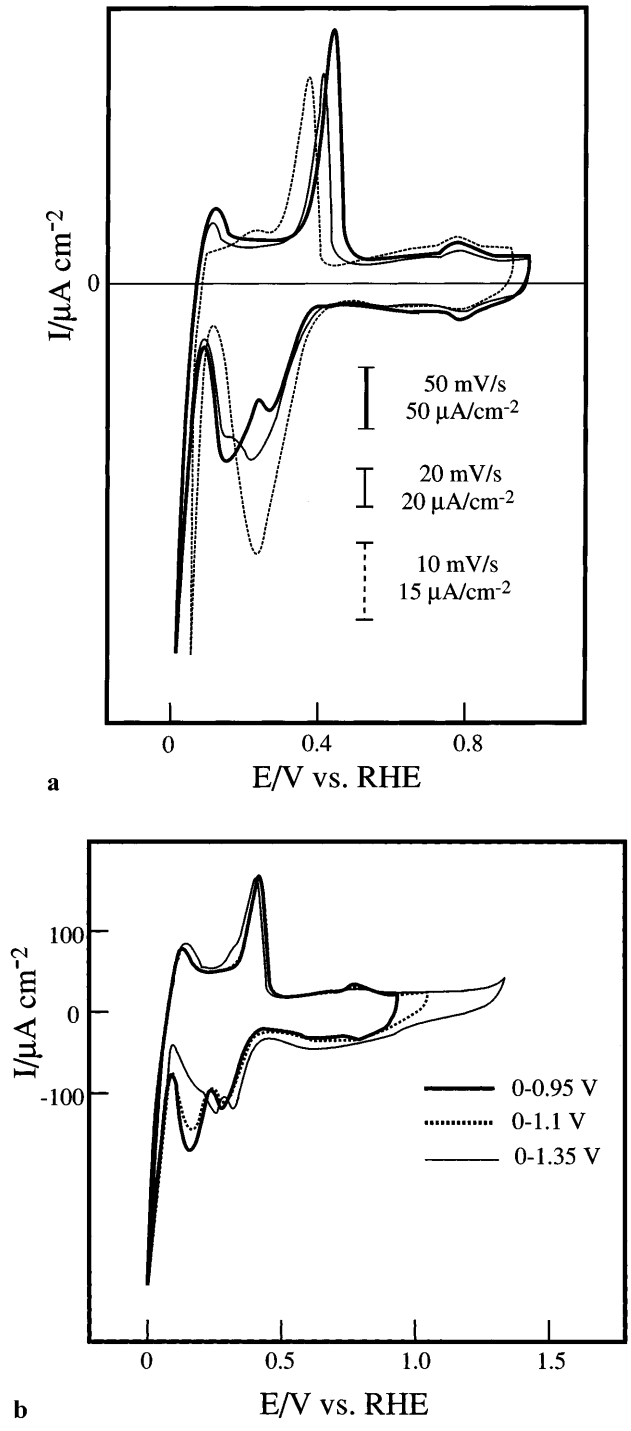

Fig. 2a, b Cyclic voltammograms for Rh(111) in 0.1 M KOH. **a** *Curves* were recorded at different potential scan rates: 50, 20 and 10 mV/s. **b** *Curves* show results of window-opening experiment, in which the positive limit of potential scan was varied. The potential scan rate was 50 mV/s

defined surface persisted in this potential range. The butterfly peaks of Rh(111) at 0.64 V in 0.1 M $HClO_4$, the signature of a long-range ordered Rh(111) surface, are also absent. The small symmetric peaks at ca. 0.75 V are thought to be related to the butterfly peaks observed more clearly in $HClO_4$ and HF.

However, it was surprising to us that the peaks observed in the potential range 0–0.5 V were asymmetric on Rh(111) in KOH even at the slowest scan rate of 10 mV/s. The cathodic peak shifted in the cathodic direction with an increase in the scan rate, splitting into two peaks at 50 mV/s. The main anodic peak shifted in the opposite direction. The appearance of the asymmetric peaks, presumably resulting from the hydrogen adsorption and desorption reaction, was not due to either contamination or disordering of the well-defined Rh(111) in 0.1 M KOH. Similar voltammetric peaks were also found in 0.1 M NaOH. A well-defined Pt(111) was examined in the same solutions as those used for Rh(111), yielding the well-known symmetric CV reported previously [3, 38]. This result indicates that the CV shown in Fig. 2a was not due to contamination in solutions. We also investigated a polycrystalline Rh electrode, with which nearly symmetric broad peaks were observed for the hydrogen adsorption and desorption reaction in the potential range 0–0.4 V. The overall shape of the CV of polycrystalline Rh was almost identical to that reported previously [36, 37]. After recording the CV shown in Fig. 2a, the electrode was transferred to and further investigated in 0.1 M $HClO_4$ or 0.1 M HF. The observed CV was identical to that shown in Fig. 1, indicating that no surface roughening was involved in the alkaline solution in the potential range shown in Fig. 2a. These results strongly suggest that the hydrogen adsorption and desorption reaction is fairly slow and kinetically controlled on the Rh(111) surface in the alkaline solution. It is noteworthy, however, that the charge consumed during the hydrogen adsorption was ca. 500 $\mu C\ cm^{-2}$, which is nearly twice as large as that (260 $\mu C\ cm^{-2}$) expected for a 1:1 ratio of hydrogen atoms to Rh atoms [21]. We expect that not only the hydrogen adsorption but also the reduction of oxygenated species might be superimposed in the peaks shown in Fig. 2a. A more detailed study is needed for further discussion about surface reactions on Rh(111) in the alkaline media.

When the voltammetric scans were extended to potentials more positive than 0.95 V, the peaks in the hydrogen adsorption region became broad and poorly defined, as shown in Fig. 2b. The change in the shape of the CV strongly suggests that the well-defined surface is roughened because of the formation of oxides [17, 21]. The surface roughening of Rh(111) was previously investigated in acidic solutions using in situ STM [21]. The quality of an Rh(111) surface was less clearly revealed by the electrochemical measurement in the alkaline solution than by in situ STM imaging, which unambiguously determines the degree of surface ordering, as described in the next section.

The addition of 1 mM KSCN vastly changed the morphology of the CV, as shown in Fig. 3a,b in 0.1 M KOH and in 0.1 M $HClO_4$, both containing 1 mM KSCN, respectively. Regardless of the acidity or alkalinity of the solution, the CVs are featureless in double-layer potential ranges, showing small charging

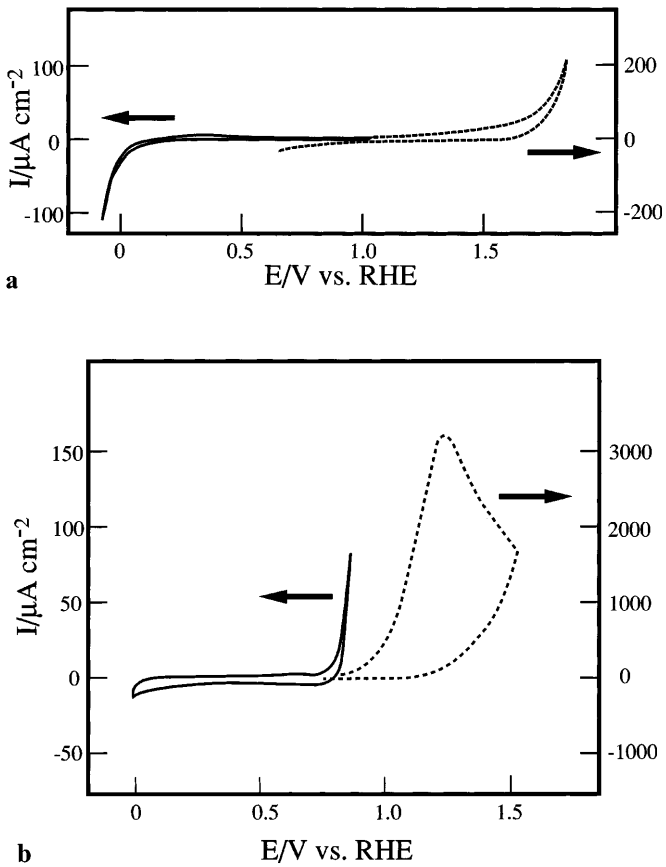

Fig. 3a, b Cyclic voltammograms for Rh(111) in the presence of KSCN in alkaline and acidic media. **a** 0.1 M KOH + 1 mM KSCN. **b** 0.1 M $HClO_4$ + 1 mM KSCN

currents only. This suggests that SCN^- ions are strongly attached to the Rh(111) surface, inhibiting the hydrogen adsorption and desorption reaction. The hydrogen evolution reaction is also slightly shifted to more negative potentials by adsorbed SCN^-. In 0.1 M KOH the anodic current begins to rise at 1.5 V, compared to 0.75 V in 0.1 M $HClO_4$. The diffusion-controlled oxidation peak at 1.3 V observed in the acidic solution is due to the electrooxidation of SCN^- ions in solution. A similar oxidation peak was previously observed on Pt(111) [34]. The anodic oxidation of thiocyanate in non-aqueous solutions was examined by IR spectroscopy, which showed the formation of thiocyanogen (NCS-SCN) in acetonitrile [26]. Thiocyanogen hydrolyzes in aqueous solutions. The electrooxidation of SCN^- ions in solution on the surface of Pt has been formulated as follows [34]:

$$SCN^- + 4H_2O = SO_4^{2-} + CN^- + 8H^+ + 6e^- \quad (1)$$

A similar reaction is expected to occur on Rh(111), although the pH dependence of the oxidation of SCN^- should be further investigated. The absence of a clear diffusion-controlled peak seen in the alkaline solution (Fig. 3a), suggests that the electrooxidation of SCN^- is more complicated than that represented by Eq. 1.

In situ STM in 0.1 M KOH

In our previous in situ STM study of Rh(111) [21–23], acid solutions such as $HClO_4$, H_2SO_4, and HF were used exclusively because of the well-characterized electrochemistry of Rh(111) in the acidic solutions. The present in situ STM observation was carried out for the first time in an alkaline solution.

Typical surface morphology of an as-prepared Rh(111) electrode is represented by the large-scale scan of a large area of 500×500 nm^2 in Fig. 4a, which reveals atomically flat terrace-step features at 0.5 V in 0.1 M KOH. All steps are monatomic (0.23 nm high), and their orientations are parallel to the close-packed direction of Rh(111) substrate. The terraces are mostly more than 100 nm wide; 150-nm wide terraces were also frequently observed. Several pits produced during the flame-annealing-quenching procedure can be seen on the atomically flat terraces shown in Fig. 4a. The densities of pits and also frequently observed islands strongly depended on experimental conditions of the surface treatment using the H_2-O_2 flame. Slower cooling was found to be more suitable for producing wider terraces with fewer pits and islands.

High-resolution STM imaging revealed the atomic structure of a bare Rh electrode, as shown in Fig. 4b. A hexagonal atomic structure can be recognized with an interatomic distance of ca. 0.27 nm. The corrugation height was typically in the range of 0.02–0.023 nm for each atom. Almost the same values were found in the acidic solutions as described previously [21–23]. The image shown in Fig. 4b clearly demonstrates that the Rh(111) surface has the (1×1) structure even in the alkaline solution. An identical atomic image was obtained in the potential range 0.1–0.6 V, indicating that either adsorbed hydrogen atoms or oxygenated species were not resolved. The surface became rough when the electrode potential was more positive than 1.0 V because of the oxidation of the surface, as expected from Fig. 2b. The atomically flat terrace-step structure disappeared after applying several potential cycles between 0.1 and 1.5 V, leaving a rolling hill structure. A similar structural change occurred in $HClO_4$, as described in our previous paper [21].

After obtaining a large-scale STM image of the bare Rh(111) in 0.1 M KOH at 0.5 V, a KSCN solution was injected. The surface morphology was not affected by the adsorption of thiocyanate. The same position and shape of monoatomic-step lines were found before and after the injection of SCN^- ions. Figure 5a shows a high-resolution STM image (obtained at 0.5 V) of the SCN^- adlayer in an area of 50×50 nm^{-2}. The appearance of large number of pits and small islands, seen in Fig. 5a, was not due to the adsorption of SCN^- but to the flame-annealing-quenching procedure described above. It is surprising that ordered atomic features are discerned both on terraces and in pits. The strong tendency of SCN^- to adsorb on Rh(111) is clearly

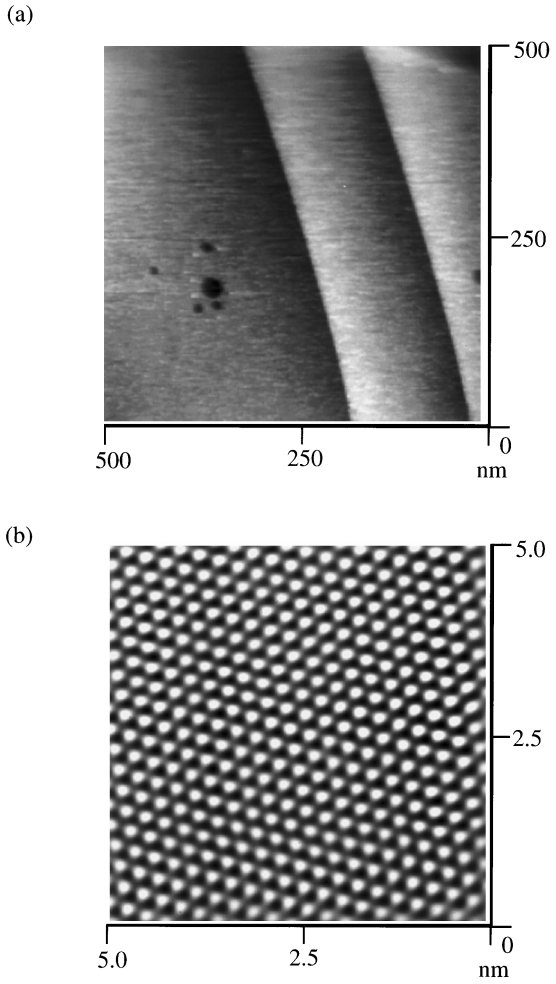

Fig. 4 STM images showing topographies, **a** on a large scale and **b** with atomic resolution, of an Rh(111) surface in 0.1 M KOH. The scan rates were 40.7 and 61 Hz and tunneling currents 10 and 20 nA for **a** and **b**, respectively

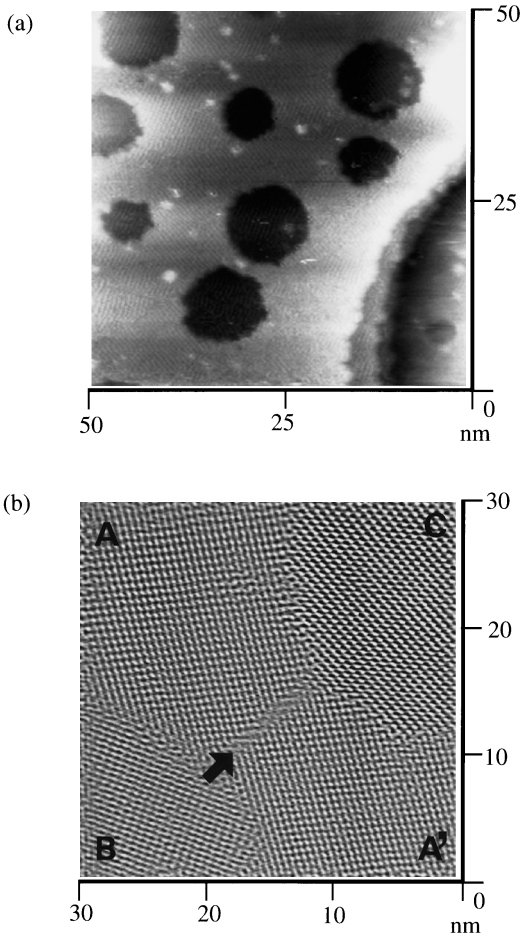

Fig. 5a, b Atomic resolution STM images of SCN^- adlayer on Rh(111) in 0.1 M KOH + 1 mM KSCN. **a** Large-scale STM image: tunneling current 10 nA and scanning rate 20.35 Hz. **b** The designated areas **A**, **B** and **C** are rotational domains. **A** and **A′** are domains of packing-fault. Tunneling current was 20 nA and scanning rate 40.7 Hz

observed. Individual bright spots exist very near the atomic steps and even on narrow terraces.

Another higher-resolution STM image of an area of 30×30 nm^2, shown in Fig. 5b, discloses ordered atomic arrays with sharply defined domain boundaries. In each domain, an atomic structure with square symmetry can be seen. The domains A, B, and C, with an identical atomic structure, exhibit 60° rotation with respect to each other, suggesting that they are rotational domains of one structure on Rh(111), with a threefold symmetry. In the meantime, the regions marked A and A′ can be classified as domains of packing-fault, in which the atomic rows are shifted by a half lattice unit with respect to each other. This result can be easily identified if one views an atomic row in domain A to A′. The arrow in Fig. 5b indicates the packing-fault boundary. The range of a single domain of the SCN^- adlayer could extend over an area as wide as 20×20 nm^2, but no particular preference of the rotational domains was noted. Three rotational domains seemed to appear with an equal probability. Figure 6a further highlights a close-up view of one of the ordered SCN^- domains. The atomic rows labeled I and II are nearly orthogonal, and two nearest neighbors are separated by 0.54 and 0.46 nm along these two directions. These distances correspond to twice and $\sqrt{3}$ times the interatomic distance for Rh atoms (0.27 nm), respectively. Furthermore, the atomic rows of I are parallel to a close-packed direction of Rh(111), while the atomic rows of II align along the $\sqrt{3}$ direction of Rh(111). These in situ STM results allow an assignment of $(2 \times \sqrt{3})$ symmetry to this structure. A corresponding unit mesh is outlined in the Figure. All protrusions exhibit an identical corrugation height (0.06 nm), so that all SCN^- anions are expected to occupy the same kind of adsorption sites. A tentative model for the $(2 \times \sqrt{3})$ structure is depicted in Fig. 6b, which corresponds to a coverage of 0.25. Note that all SCN^- anions, represented by thick circles, are assigned to on-top sites.

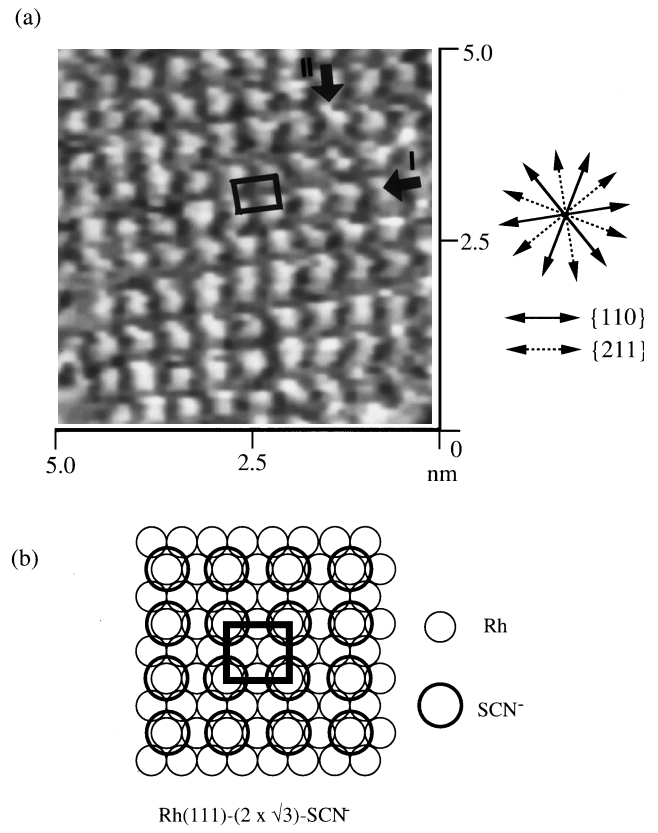

Fig. 6 a High resolution STM image showing structural details of the SCN^- adlayer on Rh(111) in 0.1 M KOH + 1 mM KSCN. Tunneling current was 5 nA and scanning rate 27.13 Hz. A $(2 \times \sqrt{3})$ unit cell is outlined in the image. **b** A ball model for the Rh(111)-$(2 \times \sqrt{3})$-SCN^- structure

Hubbard and co-workers investigated the adlayer structures of SCN^- on Pt(111) using UHV-EC, reporting at least two adlayer structures with (2×2) and, more recently, (1×2) symmetries [32–34]. The $(2 \times \sqrt{3})$ structure was not observed on Pt(111). However, it is interesting to note that a $c(2 \times \sqrt{3})$ structure with the same symmetry, denoted by $c(2 \times 4)$ in the literature [39], was reported for sulphur (S) on a Rh(111) surface UHV, although the surface coverage of S was assumed to be 0.5, twice the coverage of SCN^- in Fig. 6b. The similar symmetries observed for SCN^- and S suggest that the interaction of S with Rh(111) substrate dominates the structure, despite the lower coverage for SCN^- than for S.

We have assumed that SCN^- adsorbs predominantly with its S end, as was found by other independent studies employing UHV techniques and IR spectroscopy. In the case of Pt(111), both S-bound and N-bound configurations have been identified by means of HREELS [34]. In the present study, the effect of electrode potential on the structure of the SCN^- adlayer was carefully investigated, revealing that the same atomic structure persisted in the potential range between 0.2 and 0.8 V. No direct evidence was found for potential-dependent structural changes in the adlayer of SCN^- on Rh(111), suggesting that the S-bound configuration is predominant in the alkaline solution. However, blotches of ill-defined sizes rapidly deposited on the surface at potentials more negative than 0.1 V. These blotches seemed to grow preferentially at domain boundaries of the well-ordered $(2 \times \sqrt{3})$ structures, and continued to deposit on the surface until STM finally failed to reveal the $(2 \times \sqrt{3})$ structure. The cathodic current begins to rise at 0.1 V as shown by the CV in Fig. 3a. The cathodic current cannot be attributed solely to the evolution of hydrogen. The formation of an adlayer with the N-bound configuration as well as the reduction of SCN^- may occur in the cathodic potential range. However, the highly ordered $(2 \times \sqrt{3})$ structure was found to reappear after the potential was shifted back to 0.4 V.

In situ STM in 0.1 M $HClO_4$

We have also examined the SCN^- adlayer on Rh(111) in acidic solution (0.1 M $HClO_4$ + 1 mM KSCN). Figure 7a shows a typical atomic image obtained at 0.2 V. The atomically flat terrace was almost completely covered by adsorbed SCN^-, although many atomic defects were usually observed in STM images obtained in the acidic solution, as can be seen in Fig. 7a. However, it was not difficult to obtain high-resolution images for determining the adlayer structure. The high-resolution STM image shown in Fig. 7b clearly reveals a hexagonal arrangement with equally separated protrusions with ca. 0.54 nm spacing, which is twice the distance between Rh atoms. The atomic rows shown in Fig. 7b are parallel to the close-packed rows of Rh(111). This atomic structure was consistently observed in the potential range 0.2–0.6 V. Now, it is clear that the structure in the acidic solution is different from that observed in the alkaline solution. From the atomic image shown in Fig. 7b, we conclude that the adlayer of SCN^- has a (2×2) structure on Rh(111) in the acidic solution. A ball model corresponding to a coverage of 0.25 is depicted in Fig. 7c to reconcile the atomic resolution STM image.

This solution composition effect on the SCN^- adlayer structure comes as a surprise, because the previous UHV-EC experiments revealed an adlayer structure with (2×2) symmetry on Pt(111), showing no pH dependence. The pH dependence of the structure found on Rh(111) may suggest that SCN^- ions are more weakly bound to Rh(111). The adsorbed SCN^- ions may be protonated in the acidic solution, while cations such as K^+ are expected to be located near the SCN^- ions in the alkaline solution to compensate for the coulombic repulsion between SCN^- ions. The difference in the structure can be largely attributed to the difference in interaction between SCN^- and coadsorbed H^+ in acidic and K^+ in alkaline solutions.

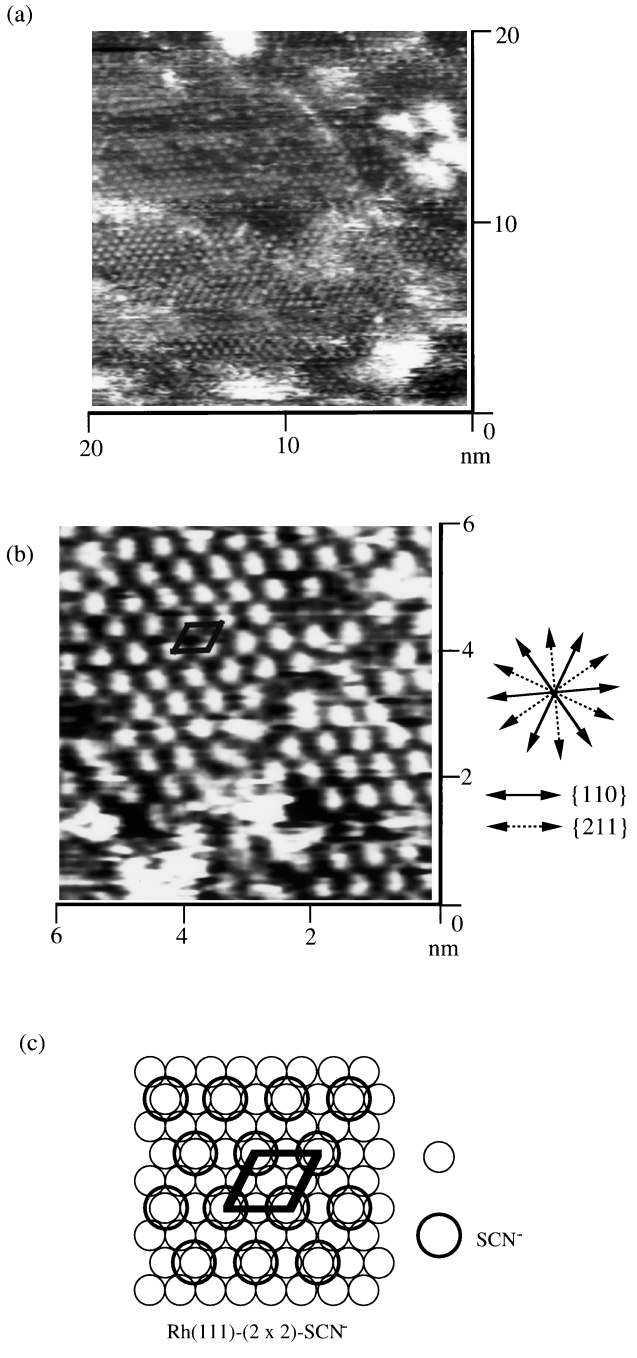

Fig. 7a, b High-resolution STM images of the SCN^- adlayer on Rh(111) in 0.1 M $HClO_4$ + 1 mM KSCN. Tunneling currents were 20 and 50 nA, and scanning rates 27.13 and 40.7 Hz for **a** and **b**, respectively. **c** A ball model for the Rh(111)-(2×2)-SCN^- structure

Finally, it should be noted that the previously proposed (2×2) structure for SCN^- on Pt(111) includes two SCN^- ions in the unit cell, resulting in a surface coverage of 0.5 [32, 33]. As shown in Fig. 7c, the unit cell on Rh(111) includes only one SCN^- ion. We did not observe an additional spot corresponding to the structure with the coverage of 0.5 proposed for Pt(111) [35]. Our preliminary in situ STM study of SCN^- on Pt(111) mostly revealed the (2×2) structure, identical to that shown in Fig. 7b. However, one of the highest-resolution images showed an additional spot in the unit cell [35]. If the additional spot is due to an adsorbed SCN^-, the STM image reported in our previous paper is completely consistent with that proposed by Hubbard and co-workers [32, 33]. Nevertheless, our present observation on Rh(111) suggests that the surface coverage of SCN^- should be 0.25 for both structures found in the acidic and alkaline solutions. N-bound species may not exist at the electrode/electrolyte interface. Such species, confirmed by HREELS, suggest that a structural transformation might have occurred in UHV.

Conclusion

High-resolution in situ STM imaging has revealed the structures of thiocyanate layers specifically adsorbed on Rh(111). Two structures, $(2 \times \sqrt{3})$ and (2×2), with the same coverage of 0.25, were identified by atomic resolution STM in alkaline and acidic solutions, respectively. The same appearances of the SCN^- anions in the STM images taken in both alkaline and acidic solutions indicate that they occupy the same kind of adsorption sites, possibly the on-top sites. The in situ STM results also suggest that S-bound species dominated, particularly in alkaline medium. In situ STM imaging of potential-dependent electrode surface structures was also demonstrated.

References

1. Yau S-L, Vitus CM, Schardt BC (1990) J Am Chem Soc 112: 3677
2. Gao X, Weaver MJ (1992) J Am Chem Soc 114: 8544
3. Yamada T, Batina N, Itaya K (1995) J Phys Chem 99: 8817
4. Yamada T, Batina N, Ogaki K, Okubo S, Itaya K (1996) In: Wieckowski A, Itaya K(eds) The Electrochemical Society, pp 43–57
5. Tanaka S, Yau S-L, Itaya K (1995) J Electroanal Chem 396: 125
6. Stuhlmann C, Villegas I, Weaver MJ (1994) Chem Phys Lett 219: 319
7. Kim YG, Yau S-L, Itaya K (1996) J Am Chem Soc 118: 393
8. Magnussen OM, Hagebock J, Hotlos J, Behm RJ (1992) Faraday Discuss Chem Soc 94: 329
9. Funtikov AM, Linke U, Stimming U, Vogel R (1995) Surf Sci 324: L343
10. Soriaga MP, Schimpf JA, Carrasquillo A Jr, Abreu JB, Temesghen W, Barriga RJ, Jeng J-J, Sashikata K, Itaya K (1995) Surf Sci 335: 273
11. Sashikata K, Matsui Y, Itaya K, Soriaga MP (1996) J Phys Chem 100: 20027
12. Ando S, Suzuki T, Itaya K (1996) J Electroanal Chem 412: 139
13. Suggs DW, Bard AJ (1994) J Am Chem Soc 116: 10725
14. Suggs DW, Bard AJ (1995) J Phys Chem 99: 8349
15. Teshima T, Ogaki K, Itaya K (1997) J Phys Chem (in press)
16. Hourani M, Wieckowski A (1988) J Electroanal Chem 244: 147

17. Hourani M, Wasberg M, Rhee C, Wieckowski A (1990) Croatica Chem Acta 63: 373
18. Rhee CK, Wasberg M, Horanyi G, Wieckowski A (1990) J Electroanal Chem 291: 281
19. Rhee CK, Wasberg M, Zelenay P, Wieckowski A (1991) Cat Lett 10: 149
20. Clavilier J, Wasberg M, Petit M, Klein LH (1994) J Electroanal Chem 374: 123
21. Wan L-J, Yau S-L, Swain GM, Itaya K (1995) J Electroanal Chem 381: 105
22. Wan L-J, Yau S-L, Itaya K (1995) J Phys Chem 99: 9507
23. Yau S-L, Kim YG, Itaya K (1996) J Am Chem Soc 118: 7795
24. Wadayama T, Sakurai T, Ichikawa S, Suetaka W (1988) Surf Sci 198: L359
25. Hatta A, Sasaki Y, Suetaka W (1986) J Electroanal Chem 215: 93
26. Foley JK, Pons S, Smith JJ (1985) Langmuir 1: 697
27. Corrigan DS, Weaver MJ (1986) J Phys Chem 90: 5300
28. Corrigan DS, Gao P, Leung LW, Weaver MJ (1986) Langmuir 2: 744
29. Corrigan DS, Foley JK, Gao P, Weaver MJ (1985) Langmuir 1: 616
30. Ashley K, Samant MG, Seki H, Philpott MR (1989) J Electroanal Chem 270: 349
31. McCarley RL, Kim YT, Bard AJ (1993) J Phys Chem 97: 211
32. Stickney JL, Rosasco SD, Salaita GN, Hubbard AT (1985) Langmuir 1: 66
33. Frank DG, Katekaru JY, Rosasco SD, Salaita GN, Schardt BC, Soriaga MP, Stern DA, Stickney JL, Hubbard AT (1985) Langmuir 1: 587
34. Cao EY, Gao P, Gui JY, Lu F, Stern DA, Hubbard AT (1992) J Electroanal Chem 339: 311
35. Yau S-L, Kim YG, Itaya K (1995) J Korean Soc Anal Sci 8: 723
36. Rakotondrainibe A, Beden B, Lamy C (1994) J Electroanal Chem 379: 455
37. Cataldi Z, Lezna RO, Giordano MC, Arvis AJ (1988) J Electroanal Chem 261: 61
38. Wagner FT, Ross PN Jr (1988) J Electroanal Chem 250: 301
39. Foord JS, Reynolds AE (1985) Surf Sci 164: 640